Meas. Sci. Technol. **23** (2012) 125204 (7pp) doi:10.1088/0957-0233/23/12/125204

Enhanced shock wave detection sensitivity for laser-produced plasmas in low pressure ambient gases using interferometry

P Hough[1,4], T J Kelly[1,4,5], C Fallon[1], C McLoughlin[1,2], P Hayden[1], E T Kennedy[1], J P Mosnier[1], S S Harilal[3] and J T Costello[1]

[1] School of Physical Sciences and NCPST, Dublin City University, Dublin 9, Ireland
[2] UMR—CNRS 6508, CRISMAT—ENSICAEN, Boulevard du Maréchal Juin, F-14050 Caen, France
[3] School of Nuclear Engineering and Center for Materials under Extreme Environment, Purdue University, West Lafayette, IN 47907, USA

E-mail: thomas.kelly9@mail.dcu.ie

Received 15 July 2012, in final form 22 October 2012
Published 20 November 2012
Online at stacks.iop.org/MST/23/125204

Abstract
We report results from the analysis of the shock wave formed following the creation of a laser-produced plasma in a gaseous atmosphere, using both interferometry and shadowgraphy. A Nomarski polarization interferometer and a focused-type shadowgraphy setup were utilized to track the evolution of the shock wave with high spatial and temporal resolution for a variety of incident laser energies and ambient gas pressures. It was found that the visibility of the shock wave was high for both techniques at high gas pressure ($\geqslant$100 mbar) and incident laser energies ($\geqslant$400 mJ). The velocity of the shock wave in these regimes was of the order of several km s^{-1}. At lower pressures ($\approx$ 1–10 mbar) and incident laser energies ($\approx$ 100–200 mJ), the visibility of the shock wave decreased dramatically and, in some cases, disappeared completely from the shadowgrams. In contrast, the shock wave remained visible in the interferograms, manifesting itself as a blurring of the fringes. The shock wave visibility was improved further by simply differentiating the interferograms to enhance the fringe boundaries. Shock velocities, exceeding 100 km s^{-1}, were detected at low background gas pressures where the enhanced shock wave visibility was provided by the interferometer.

Keywords: Nomarski interferometry, shock wave detection, shadowgraphy, laser-produced plasma

(Some figures may appear in colour only in the online journal)

1. Introduction

Since their discovery in the 1960s [1], laser-produced plasmas (LPPs) have been the focus of extensive basic research while spawning a diverse range of applications in many domains including materials growth (e.g. pulsed laser deposition) [2], materials characterization (e.g. laser-induced breakdown spectroscopy) [3], sources of ions [4] and of short wavelength light (e.g. extreme ultraviolet lithography) [5]. This research has continued apace over the years and more recently new applications of LPPs have emerged including high harmonic generation [6] and laboratory scale models of astrophysical plasmas [7].

Key to the continued success of research into, and applications of, LPPs has been the ability to effectively and accurately diagnose the properties of the plasma plume itself

[4] PH and TJK contributed equally to this work.
[5] Author to whom any correspondence should be addressed.

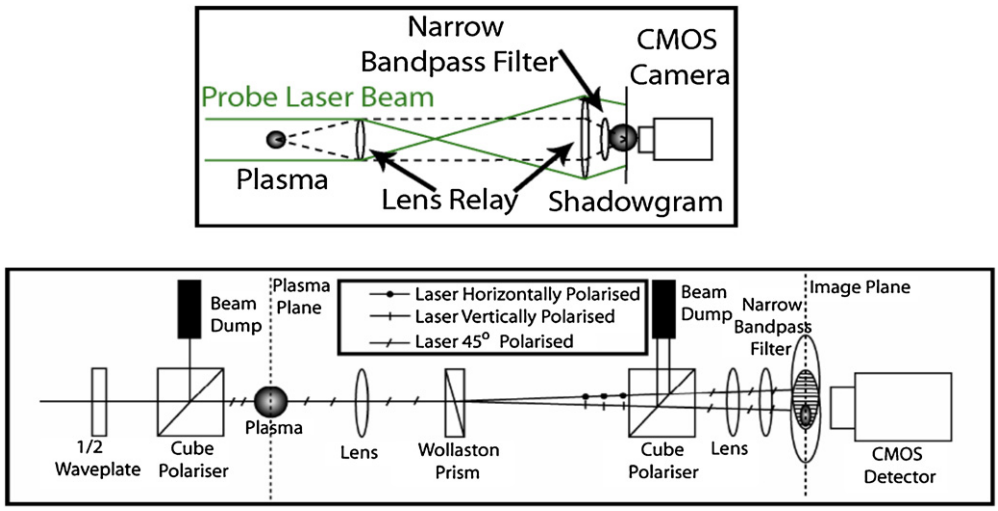

Figure 1. Experimental setup for the focused shadowgraphy and interferometry experiments.

and its interactions with its surrounding environment. A variety of diagnostic tools have been developed to diagnose the plasma plume primarily in a vacuum environment including for example, optical emission spectroscopy [8] and Thomson scattering [9], from which the electron temperatures and densities can be extracted.

A large number of applications of LPPs involve creating the plasma plume in a gaseous atmosphere, for example, pulsed laser deposition [2], micromachining [10] and nanofabrication [11] and laser-induced breakdown spectroscopy [12]. With the presence of a background gas, additional physical processes occur during laser plasma formation and expansion including, for example, shock wave creation and propagation [13], plasma confinement [14] and charge exchange [15]. Shadowgraphy is a widely established technique to probe plasma plumes induced by laser ablation in gaseous environments, especially since it offers high spatial and temporal resolution [16–20].

We report here a comparison of the visualization of laser-plasma-driven shock waves using both interferometry and shadowgraphy. Experiments were carried out in two pressure regimes, at high (100–1000 mbar) and relatively low (1–10 mbar) pressures. The expansion behaviour of the shock waves was quantitatively explored in both regimes and compared with blast wave predictions. We found that interferometry succeeded in detecting the shock waves in both regimes, whereas the shadowgraphic approach failed at low pressures.

2. Experiment

To create a single LPP, a plano-convex lens with a focal length of 300 mm and a diameter of 25.4 mm, anti-reflection coated for the 1000–1200 nm wavelength range, was used to focus output pulses from a Continuum Surelite III^{TM} Nd:YAG laser (6 ns full-width at half-maximum (FWHM) with a wavelength of 1064 nm) onto a solid slab of 99.99% pure aluminium. The spot size achieved with this optical arrangement was $\approx 100\,\mu$m and laser energies of 100, 200, 400 and 600 mJ produced peak on-target irradiances of ≈ 0.2, 0.4, 0.8 and 1×10^{12} W cm^{-2}, respectively.

A synchronized Continuum Surelite I^{TM} laser, operating at its frequency-doubled wavelength of 532 nm, with a pulse width of 4 ns (FWHM) provided the probe light source for both the Nomarski polarization interferometer and the shadowgraphy setups. Briefly, the Surelite I^{TM} probe laser was synchronized to the incoming plasma generating laser (Surelite III^{TM}) with a maximum temporal jitter of ± 1 ns. A synchronized complementary metal oxide semiconductor (CMOS) camera captured the resulting interferogram of the LPP. The delay between the plasma generating laser and both the probe laser and the camera could be varied to interrogate the plasma plume at different times during its evolution. The experimental setup for the shadowgraphy experiment is shown in figure 1 and is a so-called focused shadowgraphy arrangement [20].

Referring to figure 1, a relay lens imaged the plasma plane onto the detector plane. The incoming probe laser beam constituted the light source for the formation of each shadowgram. A narrow bandpass filter with a peak transmission wavelength of 532 nm rejected broadband optical emission from the plasma whilst permitting the probe beam to reach the detector. The Nomarski interferometer, shown in the lower part of figure 1, is a polarization-type interferometer where the spatial variation in the electron density is manifested as a phase shift of interference fringes [21].

A high precision gas flowmeter was used to introduce 99.99% pure O_2 into the vacuum chamber and the flow rate was adjusted to vary the background pressure in the chamber between 1 and 100 mbar. The experiments at a background pressure of 1000 mbar were performed in air. The similarities between O_2 and N_2 in terms of mass and specific heat ratio ensure that the background environments of air and O_2 are comparable. The Al target was mounted on a high precision in-vacuum motorized *X*–*Z* stage and was moved to reveal a fresh surface after each laser shot.

3. Results and discussion

Interferometric and shadowgraphic experiments were performed on LPPs for a variety of incident laser energies and

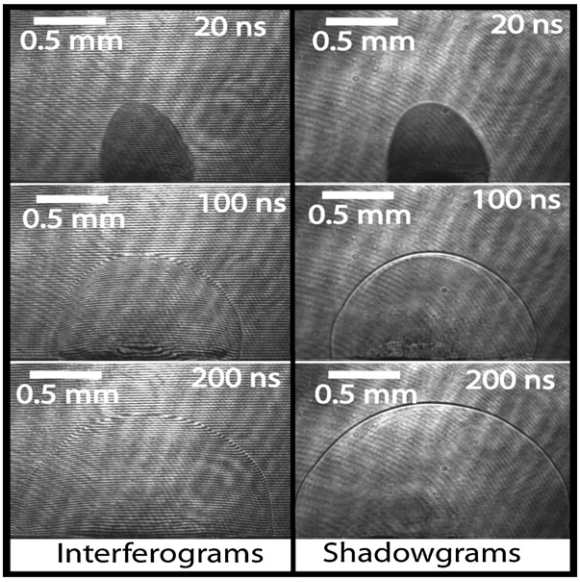

Figure 2. Comparison of interferograms (left panels) with shadowgrams (right panels) at three different time delays; 20, 100 and 200 ns following the peak of the plasma producing laser pulse. The incident laser beam had an energy of 100 mJ and the background air pressure was 1000 mbar.

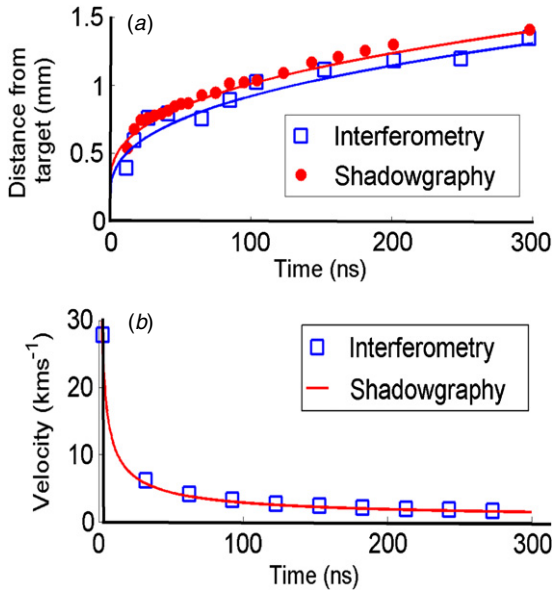

Figure 3. (*a*) Comparison of the spatio-temporal evolution of the front of the shock wave as observed using interferometry (blue) and shadowgraphy (red) along with fits from the general blast wave theory equation ($R = at^b + R_o$) which yield $R = (0.13 \pm 0.02)t^{0.4\pm0.1} + 0.22$ (from interferometry) and $R = (0.14 \pm 0.02)t^{0.4\pm0.1} + 0.26$ (from shadowgraphy). (*b*) Corresponding behaviour of the velocity of the shock front extracted from the interferometric (blue) and shadowgraphic (red) fits. The computed velocity curves are almost identical and so the interferometry velocity is represented by blue squares. These data represent plasma expansion into air at a pressure of 1000 mbar.

background gas pressures. A comparison of interferograms and shadowgrams for plasma plume expansion into air at three different delay times (20, 100 and 200 ns) following the peak of the plasma producing laser pulse is presented in figure 2. The incident 1064 nm laser pulse had an energy of 100 mJ and was focused onto the surface of a flat slab of Al to a spot of approximately 100 μm diameter in air at a pressure of 1000 mbar.

The shock wave is clearly visible in both the interferograms and shadowgrams. The spatio-temporal evolution of the shock front has been extracted from the images obtained using both diagnostic techniques. These results are plotted in figure 3(*a*) where the position of the shock front (normal to the centre of the target) is plotted as a function of time delay following plasma creation. The shock front is tracked for varying delay times between 5 and 300 ns from the interferograms (blue) and shadowgrams (red).

As can be seen from figure 3(*a*), both techniques work well in this relatively high background pressure and incident laser energy regime and show a consistent behaviour in the spatio-temporal evolution of the shock front. The errors on the prefactor (≈10%) and on the exponent (≈25%) have been determined directly from the least-squares fitting routine and are consistent across all experiments. According to the Taylor–Sedov theory [22] of blast wave propagation from a point explosion, the position of the shock front, R, at any time t, can be found from the following equation:

$$R = \zeta_o \left(\frac{E_o}{\rho_o}\right)^{\frac{1}{n+1}} t^{\frac{2}{n+2}}, \tag{1}$$

where t is the delay time following ignition, ρ_o is the background gas density, E_o is the amount of energy released during the explosion and ζ_o is a constant determined by the gas specific heat ratio.

The general form of the equation can be written:

$$R = at^b, \tag{2}$$

where b is equal to $2/(n+2)$ and $n = 3$, 2 or 1 for spherical, cylindrical or plane wave shock wave propagation, respectively [23]. These n values correspond respectively to b values of 0.40 (spherical), 0.50 (cylindrical) and 0.667 (plane). In fitting equation (2) to our data, we have used the form $R = at^b + R_o$, where R_o is a fitted parameter that we include to account for any systematic offset in the data. It is clear from figure 3 that the form of the general blast wave equation ($R = at^b + R_o$) describes the expansion dynamics of the shock wave well in our case. The experimental b value of 0.4 is in good agreement with a spherical expansion behaviour. The scale of the shock wave observations extend out to 1.4 mm which is substantially greater than the focal spot size of the laser pulse. It is noteworthy from figure 2 that the shape of the shock wave evolves as it expands into the gas. Measurements of the ratio of the radii normal and parallel to the target surface show that it becomes notably more spherical in nature as the time increases.

Shown in figure 3(*b*) is the temporal evolution of the velocity of the shock front obtained from an analysis of the interferograms (blue) and shadowgrams (red). The interferometry data are generally consistent with that from shadowgraphy. These results are also consistent with those of related experiments published in the literature, e.g. [24–26].

It is also clear from figures 2 and 3 that interferometry can be utilized to diagnose the spatio-temporal development

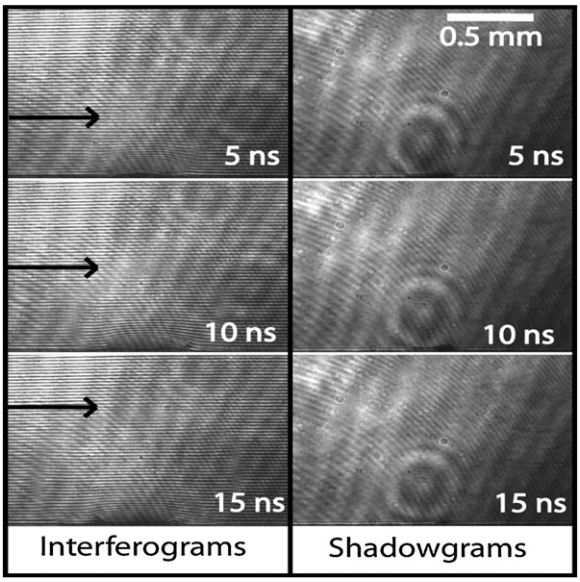

Figure 4. Comparison of interferometry (left panels) with shadowgraphy (right panels) of a laser-produced aluminium plasma expanding into a background gas of oxygen maintained at a pressure of 10 mbar for three different time delays following the peak of the pump laser pulse, namely 5, 10 and 15 ns. The black arrows in the interferograms indicate the position of the compressive gas layer.

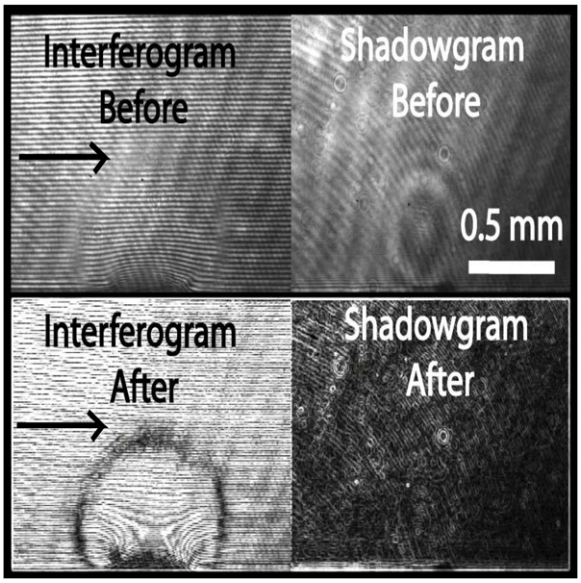

Figure 5. Comparison of the interferograms (left) and shadowgrams (right) from figure 4 before and after the application of the 'find edges' algorithm in the ImageJ software package for images taken at a time delay of 10 ns and a background pressure of 10 mbar.

of the compressive gas layers formed when plasmas expand into background gases, just as effectively as shadowgraphy. Our experiments however show (see below) limitations to the shadowgraphic technique when the background gas pressure becomes relatively low (defining low background gas pressure here as lying between ≈1 and 10 mbar). In this rarefied gas case, the compressive gas layer becomes less well defined as a result of reduced compression at the plasma–gas interface. Hence, the variation in the refractive index at the shock front decreases and so it becomes more difficult to detect. For shadowgraphy, the concomitant redistribution of image brightness due to the change in the refractive index is much less abrupt and hence it struggles to detect shock waves induced by plasmas expanding into lower background gas pressure regimes. The redistribution in image brightness is related to the second derivative of the refractive index of the plasma [27] and so it is not too surprising that the visibility of the shock front at low pressure can drop below the minimum detectable contrast of the shadowgraphy system. We present in figure 4 results from an experiment in which both interferometery and shadowgraphy were performed on a LPP expanding into O_2 at a pressure of 10 mbar. The energy of the incident laser beam was 100 mJ as before.

Looking at figure 4, there appears to be no evidence of a compressive gas layer at the plasma–gas interface in the shadowgrams (right hand panels). On the other hand, on very close inspection, the interferograms (left hand panels) display some slight evidence of a shockfront (albeit extremely weak), manifested as a blurring of the fringes all around the locus of the shockfront. The black arrows on the figure point to the apex of this locus. It has to be admitted that this fringe blurring is very difficult to observe in the raw images, especially in print. However, it is possible to significantly enhance the signature of the shock front by employing a simple 'find edges'-type algorithm which brings into sharp relief the discontinuities in image contrast caused by the fringe blurring. This is achieved by differentiating the image using a first-order Sobel operator [28]. A freeware software package 'ImageJ' [29] was employed to perform the image processing during this study. Figure 5 shows a comparison of the interferogram and shadowgram from figure 4, prior to and following the application of this operator for the images recorded at a time delay of 10 ns. The black arrows from figure 4 are reproduced here to aid the reader in comparing figures 4 and 5.

The algorithm enhances the visibility of the blurred fringes at the position of the compressive gas layer or shock-wavefront. There appears to be no evidence of this feature in the shadowgram, either following the application of the algorithm or with any further image processing (e.g. background subtraction). Using the interferometric method in these pressure regimes (where the shadowgraphy technique begins to fail), we have been able to extract the spatio-temporal evolution of the front of the compressive gas layer at low pressures. We do this for times ranging from 5 to 50 ns and present the results in figure 6. Figure 6(a) shows the expansion of the shock wave, in this low-pressure regime, as a function of time, fitted again with the formula ($R = at^b + R_o$), while figure 6(b) shows the extracted velocity–time profile. Comparing figure 6 (100 mJ incident laser pulse with a background pressure of 10 mbar) to figure 3 (100 mJ incident laser pulse with a background pressure of 1000 mbar), it is clear that the velocity of the shock wave in the background gas pressure of 10 mbar is much higher.

The shock front present in 1000 mbar pressure background gas remains in the field of view of the interferogram up to a time delay of at least 200 ns after the peak

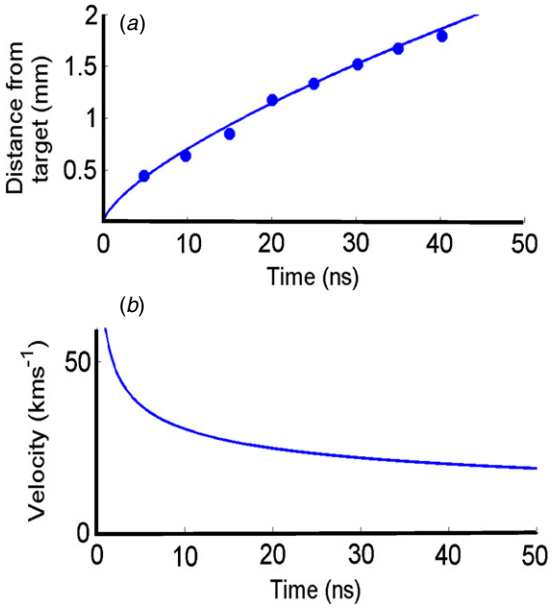

Figure 6. Spatio-temporal evolution of the compressive layer obtained from interferograms for times ranging from 5 to 50 ns (10 mbar). (*a*) Distance versus time plot of the peak position of the compressive layer between 5 and 40 ns following the peak of the pump laser pulse. Also shown is a best fit (general blast wave theory equation) to the data ($R = (0.13 \pm 0.01)t^{0.7\pm0.2} - 0.00$). (*b*) Velocity of the compressive layer (extracted from the fitted curve in top panel).

of the plasma producing laser pulse (cf figure 2). In contrast, at a pressure of 10 mbar, the high speed of the shock wave results in the interferogram remaining in the field of view of the camera only for a few tens of nanoseconds.

The results of an interferometric analysis of the spatio-temporal expansion of compressive gas fronts for a variety of background gas pressures regimes (O_2 at pressures of 1, 10 and 100 mbar) and incident laser energies (200 and 400 mJ) are presented below in figure 7. The analysis could not be performed with the shadowgraphy technique in these pressure regimes.

Table 1. Summary of the fitting results for the experiment described in figure 7.

Gas pressure	200 mJ	400 mJ
100 mbar	$a = 0.17, b = 0.6$	$a = 0.24, b = 0.6$
10 mbar	$a = 0.22, b = 0.6$	$a = 0.36, b = 0.5$
1 mbar	$a = 0.46, b = 0.48$	$a = 0.6, b = 0.6$

It is interesting to note the much lower deceleration of the shock wave in the lower pressure regime compared to the behaviour at high pressures, as shown by the comparisons of the temporal behaviour of figure 3 with those of figures 6 and 7. Furthermore, the experimental b values ranging from 0.70 to 0.48 for figures 6 and 7 are more in keeping with the planar (0.667) and cylindrical (0.50) predictions of the blast wave model, than the spherical wave ($b = 0.4$) observed at high pressures. Table 2 presents a comparison of the visibility of the shock front from interferometery and shadowgraphy for a variety of pressure and laser energy regimes. It is worth pointing out that it was not possible to perform certain experiments (more specifically, experiments with a background pressure of 1000 mbar and a laser energy $\geqslant$200 mJ) due to the breakdown of the gas itself inside the test chamber. These experiments are indicated in table 2.

It is clear that there is a wide background gas pressure range and incident laser energy parameter regime where interferometry can provide valuable insights into the propagation dynamics of the LPPs in background gases. We suggest that the combination of interferometry with

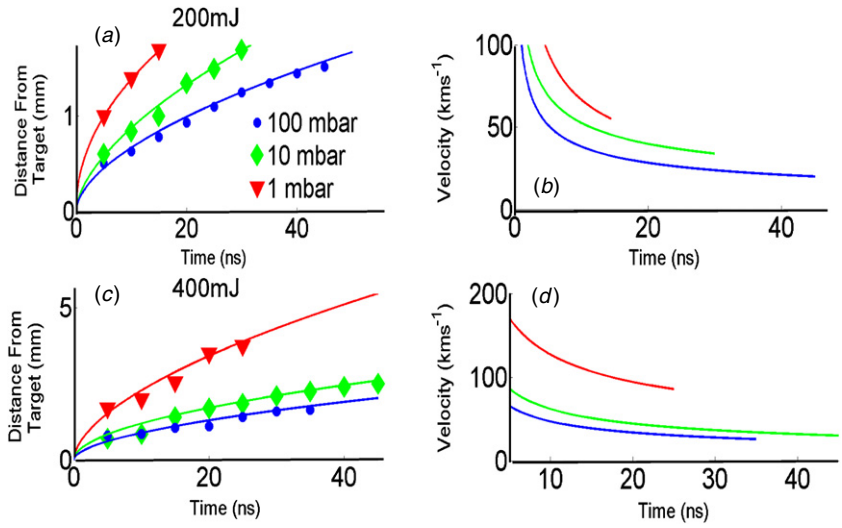

Figure 7. Spatio-temporal analysis of the compressive layer for gas pressures of 1, 10 and 100 mbar of O_2 at laser energies of 200 and 400 mJ. (*a*) Evolution of the shock front position as a function of time for an incident laser energy of 200 mJ and background O_2 pressure of 1 mbar (best fit $R = (0.46 \pm 0.07)t^{0.48\pm0.18} + 0.00$), 10 mbar (best fit: $R = (0.22 \pm 0.02)t^{0.6\pm0.2} + 0.00$) and 100 mbar (best fit: $R = (0.17 \pm 0.02)t^{0.6\pm0.2} - 0.00$). (*b*) Extracted velocity profiles from best curve fits in (*a*). (*c*) Temporal evolution of the compressive gas layer for an incident laser energy of 400 mJ and background gas pressures of 1 mbar of O_2 (best fit: $R = (0.6 \pm 0.07)t^{0.6\pm0.2} + 0.00$), 10 mbar (best fit: $R = (0.36 \pm 0.04)t^{0.5\pm0.2} + 0.00$) and 100 mbar (best fit: $R = (0.24 \pm 0.03)t^{0.6\pm0.2} + 0.00$). (*d*) Extracted velocity profiles from best fits in (*c*). The results of the fitting are summarized in table 1.

Table 2. Comparison of the visibility of the compressive gas layer using interferometry and shadowgraphy for various experimental parameters. Legend: ✓ = visible, × = not visible, – = experiment not possible (due to gas breakdown).

Gas pressure	Diagnostic	100 mJ	200 mJ	400 mJ	600 mJ
1 mbar (O_2)	Interferometry	✓	✓	✓	✓
	Shadowgraphy	×	×	×	×
10 mbar (O_2)	Interferometry	✓	✓	✓	✓
	Shadowgraphy	×	×	×	✓
100 mbar (O_2)	Interferometry	✓	✓	✓	✓
	Shadowgraphy	×	×	✓	✓
1000 mbar (air)	Interferometry	✓	–	–	–
	Shadowgraphy	✓	–	–	–

appropriate image processing is a useful addition to the existing range of laser diagnostic tools for gas dynamics studies in laser plasma–gas collisions experiments at low ambient pressures.

4. Conclusions

We have directly compared the capabilities of shadowgraphy and interferometry to visualize and analyse the propagation dynamics of shock waves formed by creating a laser-produced plasma in a background gas. It was found that the compressive layer was visible in both shadowgraphy and interferometery for high background gas pressures (≈100–1000 mbar) and the spatio-temporal analysis of the layer using both techniques gave similar results. The velocity of the expansion of the compressive gas layer was relatively low at these pressures (approximately tens of km s^{-1}). When the pressure of the background gas was lowered, however, to the range 1–10 mbar, the compressive gas layer was no longer detectable using shadowgraphy. Of the two techniques, only interferometry, combined with image edge detection, was capable of detecting the compressive layer in these background gas pressure regimes. The compressive layer had a much higher expansion velocity (exceeding 100 km s^{-1} in some cases) and manifested itself as a blurring of the fringes in the interferogram. This blurring of the fringes was visible (albeit with difficulty) in the raw interferograms, but, with close inspection, it could be detected as a small modulation in image contrast. The application of a 'find edges' algorithm clearly revealed the compressive gas layer. We propose this combination as a useful laser diagnostic for dynamic plasma–gas interactions at low gas pressure. The interferometric approach allowed a comparison of the shock wave behaviour at low and high pressures with predictions of the blast wave model.

Acknowledgments

This work was sponsored by the Science Foundation Ireland under SFI PI grant no. 07/IN.1/I1771 and the HEA PRTLI IV and V INSPIRE programs of the Second National Development Plan program (NDP2). Four of the authors (PH, TJK, PH, CMc) would like to acknowledge support from the Embark, Empower and Inspire Fellowship/Scholarship Schemes of the Irish Research Council for Science Engineering and Technology (IRCSET). SSH acknowledges funding from the DCU International Visiting Fellows Programme. The work is associated with EU COST Action MP0601 and the Erasmus Mundus Joint Doctorate 'EXTATIC'. The authors wish to thank Des Lavelle for help in the design and construction of the experimental system.

References

[1] Hughes T P 1975 *Plasmas and Laser Light* (London: Adam Hilger)
[2] O'Haire R, McGlynn E, Henry M O and Mosnier J P 2007 ZnO nanostructured thin films grown by pulsed laser deposition in mixed O_2/Ar background gas *Superlattice Microstruct.* **42** 468–72
[3] Khater M A, Costello J T and Kennedy E T 2002 Optimization of the emission characteristics of laser-produced steel plasmas in the vacuum ultraviolet: significant improvements in carbon detection limits *Appl. Spectrosc.* **56** 970–83
[4] Yeates P, Costello J T and Kennedy E T 2010 The DCU laser ion source *Rev. Sci. Instrum.* **81** 043305
[5] Hayden P, Cummings A, Murphy N, O'Sullivan G, Sheridan P, White J and Dunne P 2006 13.5 nm extreme ultraviolet emission from tin based laser produced plasma sources *J. Appl. Phys.* **99** 093302
[6] Ganeev R A, Suzuki M, Baba M and Kuroda H 2009 Extended high-order harmonics from laser-produced Cd and Cr plasmas *Appl. Phys. Lett.* **94** 051101
[7] Farley D R, Estabrook K G, Glendinning S G, Glenzer S H, Remington B A, Shigemori K, Stone J M, Wallace R J, Zimmerman G B and Harte J A 1999 Radiative jet experiments of astrophysical interest using intense lasers *Phys. Rev. Lett.* **83** 1982–5
[8] Hafeez S, Shaikh N M and Baig M A 2008 Spectroscopic studies of Ca plasma generated by the fundamental, second, and third harmonics of a Nd:YAG laser *Laser Part. Beams* **26** 41–50
[9] Froula D H, Ross J S, Divol L and Glenzer S H 2006 Thomson-scattering techniques to diagnose local electron and ion temperatures, density, and plasma wave amplitudes in laser produced plasmas *Rev. Sci. Instrum.* **77** 10E522
[10] Bartnik A, Fiedorowicz H, Jarocki R, Kostecki J, Rakowski R, Szczurek A and Szczurek M 2010 Micro- and nanoprocessing of polymers using a laser plasma extreme ultraviolet source *Acta Phys. Pol.* A **117** 384–90
[11] Kabashin A V, Delaporte P, Pereira A, Grojo D, Torres R, Sarnet T and Sentis M 2010 Nanofabrication with pulsed lasers *Nanoscale Res. Lett.* **5** 454–63
[12] Pasquini C, Cortez J, Silva L M C and Gonzaga F B 2007 Laser induced breakdown spectroscopy *J. Braz. Chem. Soc.* **18** 463–512
[13] Geohegan D B 1992 Fast intensified-CCD photography of $YBa_2Cu_3O_{7-x}$ laser ablation in vacuum and ambient oxygen *Appl. Phys. Lett.* **60** 2732–4
[14] Amoruso S, Schou J and Lunney J G 2006 Multiple-scattering effects in laser ablation plume propagation in gases *Europhys. Lett.* **76** 436–42
[15] Henc-Bartolic V, Andreic Z, Gracin D, Aschke L, Ruhl F and Kunze H J 1998 Spectral line enhancement in laterally colliding boron-nitride plasmas *Phys. Scr.* T **75** 297–9
[16] Okano Y, Hironaka Y, Nakamura K G and Kondo K 2003 Time-resolved electron shadowgraphy for 300 ps laser ablation of a copper film *Appl. Phys. Lett.* **83** 1536–8
[17] Whitty W and Mosnier J P 1998 Diagnostic of an expanding laser-produced lithium plasma using ICCD frame

photography and shadowgraphy *Appl. Surf. Sci.* **127–129** 1035–40
[18] Siew W O, Tou T Y and Wong K H 2005 Shadowgraphy of pulsed CO_2 laser ablation of polymers *Appl. Surf. Sci.* **248** 281–5
[19] Gravel J Y and Boudreau D 2009 Study by focused shadowgraphy of the effect of laser irradiance on laser-induced plasma formation and ablation rate in various gases *Spectrochim. Acta* B **64** 56–66
[20] Settles G S 2001 *Schlieren and Shadowgraph Techniques: Visualizing Phenomena in Transparent Media* (Berlin: Springer)
[21] Hough P, McLoughin C, Kelly T J, Hayden P, Harilal S S, Mosnier J P and Costello J T 2009 Electron and ion stagnation at the collision front between two laser produced plasmas *J. Phys. D: Appl. Phys.* **42** 055211
[22] Hutchens G J 2000 Approximate near-field blast theory: a generalized approach *J. Appl. Phys.* **88** 3654
[23] Jeong S H, Greif R and Russo R E 1998 Propagation of the shock wave generated from excimer laser heating of aluminum targets in comparison with ideal blast wave theory *Appl. Surf. Sci.* **127–129** 1029–34
[24] Thiyagarajan M and Scharer J 2008 Experimental investigation of ultraviolet laser induced plasma density and temperature evolution in air *J. Appl. Phys.* **104** 013303
[25] Porneala C and Willis D A 2009 Time-resolved dynamics of nanosecond laser-induced phase explosion *J. Phys. D: Appl. Phys.* **42** 155503
[26] Veloso F, Chuaqui H, Aliaga-Rossel R, Favre M, Mitchell I H and Wyndham E 2006 Laser-produced annular plasmas *Rev. Sci. Instrum.* **77** 063506
[27] Hutchinson I H 2002 *Principles of Plasma Diagnostics* 2nd edn (Cambridge: Cambridge University Press)
[28] Find edges algorithm in ImageJ http://rsbweb.nih.gov/ij/docs/menus/process.html
[29] Image processing and analysis in Java http://rsbweb.nih.gov/ij/